Magnetic Resonance Materials in Physics, Biology and Medicine
https://doi.org/10.1007/s10334-017-0661-9

RESEARCH ARTICLE

Segmental biventricular analysis of myocardial function using high temporal and spatial resolution tissue phase mapping

Marius Menza[1] · Daniela Föll[2] · Jürgen Hennig[1] · Bernd Jung[3]

Received: 18 May 2017 / Revised: 13 October 2017 / Accepted: 30 October 2017

Abstract

Objective Myocardial dysfunction of the right ventricle (RV) is an important indicator of RV diseases, e.g. RV infarction or pulmonary hypertension. Tissue phase mapping (TPM) has been widely used to determine function of the left ventricle (LV) by analyzing myocardial velocities. The analysis of RV motion is more complicated due to the different geometry and smaller wall thickness. The aim of this work was to adapt and optimize TPM to the demands of the RV.

Materials and methods TPM measurements were acquired in 25 healthy volunteers using a velocity-encoded phase-contrast sequence and kt-accelerated parallel imaging in combination with optimized navigator strategy and blood saturation. Post processing was extended by a 10-segment RV model and a detailed biventricular analysis of myocardial velocities was performed.

Results High spatio-temporal resolution ($1.0 \times 1.0 \times 6$ mm^3, 21.3 ms) and the optimized blood saturation enabled good delineation of the RV and its velocities. Global and segmental velocities, as well as time to peak velocities showed significant differences between the LV and RV. Furthermore, complex timing of the RV could be demonstrated by segmental time to peak analysis.

Conclusion High spatio-temporal resolution TPM enables a detailed biventricular analysis of myocardial motion and might provide a reliable tool for description and detection of diseases affecting left and right ventricular function.

Keywords Right ventricle · Tissue Phase Mapping · Phase-contrast velocity mapping · Biventricular analysis

Introduction

Right ventricular function determines prognosis in patients with a variety of heart diseases [1]. Imaging of the right ventricle (RV) by echocardiography is restricted to the acoustic windows so that MRI has become the gold standard for analysis of global RV function such as right ventricular ejection fraction. However, the assessment of regional motion parameters of the RV might have several advantages over the analysis of global function. For example, segmental parameters might help to diagnose RV disease at earlier stages [2]. In addition, segmental RV function analysis is an important tool for the evaluation of cardiac resynchronization [3]. It has been demonstrated that segmental RV myocardial velocities correlate with ejection fraction in healthy and diseased RV [4]. In contrast to MR tagging, which is limited in imaging of the thin RV walls due to the spatial restriction of the tagging grids, phase-contrast MRI permits a detailed assessment of regional myocardial velocities in all spatial directions and with high spatial coverage of the entire heart. Phase-contrast MRI in the context of velocity mapping of the myocardium is typically referred to as tissue phase mapping (TPM).

TPM has been widely used in volunteer and patient studies for the investigation of left-ventricular (LV) myocardial velocities [5–8] and has been validated in various publications with the result of a good agreement and higher reproducibility compared to other modalities such as tissue doppler imaging (TDI) [9–12]. Because of a mean LV myocardial wall thickness of about 7–10 mm [13–15], typical

✉ Marius Menza
marius.menza@uniklinik-freiburg.de

[1] Department of Radiology, Medical Physics, Medical Center - University of Freiburg, Faculty of Medicine, University of Freiburg, Breisacher Straße 60a, 79106 Freiburg, Germany

[2] Department of Cardiology and Angiology I, Heart Center - University of Freiburg, Faculty of Medicine, University of Freiburg, Freiburg, Germany

[3] Institute of Diagnostic, Interventional and Pediatric Radiology, University Hospital Bern, Bern, Switzerland

Published online: 15 November 2017

spatial resolutions range from about 1.3 mm in frequency encoding direction to about 3.4 mm in phase encoding direction. Data acquisition is usually performed within breathhold [6, 8, 16, 17] or during free breathing with navigator respiration control [18–24]. As early as 2000, Kayser et al. presented first measurements of global and regional RV function using TPM [25]; however, with limited temporal (50 ms) and spatial resolution (2.0 × 2.3 mm).

Because of the substantially smaller RV wall thickness of about 3–5 mm [26–28], the spatial resolution of TPM needs to be increased to avoid partial volume effects during segmentation and to properly quantify myocardial velocities. Therefore, a direct adaption of data acquisition parameters as used in previous LV studies [8, 18, 29–32] seems not suitable for the RV assessment. Furthermore, a direct translation of the assessment strategy for LV TPM data is not practicable, as the right ventricle cannot be assumed as a ring, and needs to be modified according to the RV. Thus, the aim of this study is to investigate a number of modifications which are essential for a robust RV assessment: optimization of the black blood saturation pulse, the navigator respiration control, and particularly a thorough post-processing and analysis of RV myocardial velocities. With this newly developed TPM protocol, measurements and subsequent quantitative biventricular analysis of velocities and timing were performed in a volunteer cohort.

Materials and methods

Study population and data acquisition

Measurements were performed in 25 healthy volunteers (age = 29 ± 4 years, 11 female, 14 male) on a 3 T whole body system (Trio, Siemens, Erlangen, Germany) using a 12 channel thorax coil and the system spine array coil for signal reception. The study was approved by the local ethics committee, and informed consent was obtained from all participants. Standard CINE short-axis slices covering the complete LV and RV were acquired with a FLASH sequence in order to perform a standardized volumetric assessment of the LV and RV. For TPM measurements, three short-axis slices (basal, mid-ventricular, apical: positioned equidistantly with individual slice distances depending on the heart size; Fig. 1) were acquired using a navigator-controlled, prospectively ECG-gated, black blood prepared, velocity encoded phase-contrast gradient echo sequence (TE = 4.5 ms, TR = 7.1 ms, flip angle: 15°, bandwidth: 460 Hz, FOV: 352 × 264 mm^2, ACQ-Matrix: 352 × 264) with a real spatial resolution of 1.0 × 1.0 × 6 mm^3 and a velocity sensitivity (*venc*) of 15 cm/s in-plane and 25 cm/s through-plane. To achieve a temporal resolution of 21.3 ms a sequential acquisition strategy [23] for velocity encoding was used with three k-space lines acquired per cardiac frame.

Furthermore, kt-GRAPPA based acceleration (PEAK-GRAPPA [33] with an optimized kernel structure as described by Bauer et al. [19]) with 20 auto-calibration lines and a reduction factor of $R = 5$ ($R_{net} = 3.8$) was used resulting in an acquisition time of 3.1 min (assuming an average navigator efficiency of 50% and a heart rate of 60 bpm).

Center navigator strategy

Typically, navigator echoes are acquired at the end of the CINE train and a single navigator decides about the acceptance of the subsequent cardiac cycle [34]. In this work the navigator echo was recorded in the middle of the cardiac cycle (after half of the number of cardiac frames). This has the advantage that the acquisition of the current breathing position is temporally closer (± 0.5 heartbeat (HB) vs + 1 heartbeat) to the data of interest, which is either rejected or accepted depending on the position of the diaphragm. Both navigator schemes are illustrated in Fig. 2a.

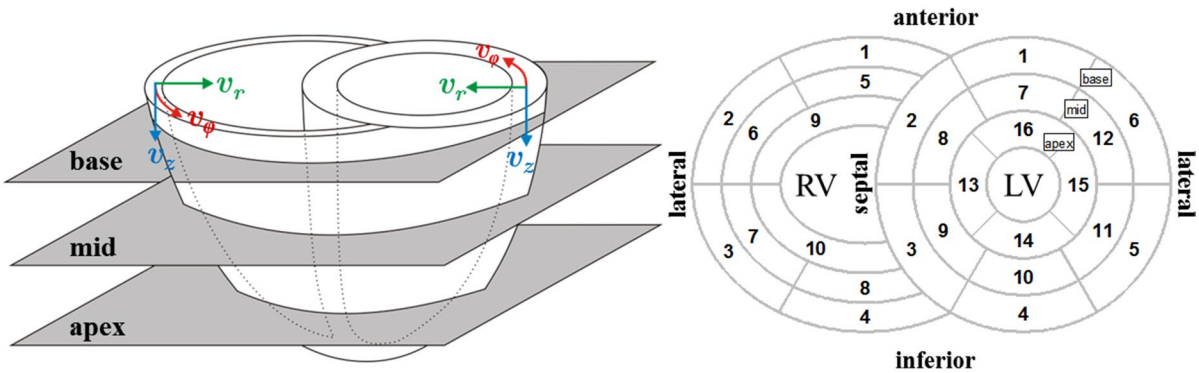

Fig. 1 Left: schematic illustration of slice locations and in-plane velocity calculation; right: extended left-ventricular American Heart Association 16-segment model with additional self-defined 10-segment model of the right ventricle illustrated in a bullseye plot

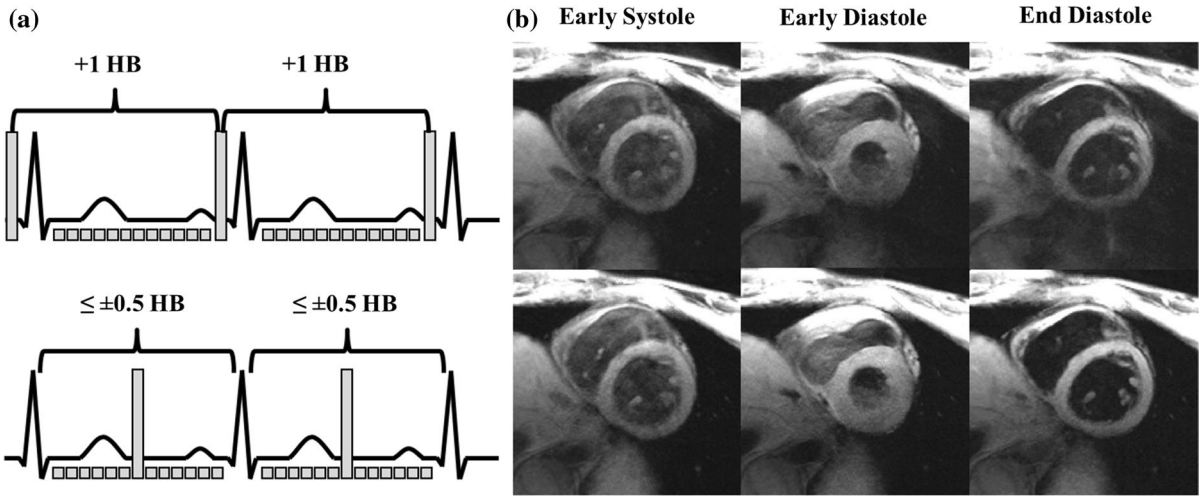

Fig. 2 **a** Application and decision scheme of the conventional prospective navigator (top) and the proposed center navigator strategy (bottom): the conventional navigator echo located at end of cardiac cycle deciding about data from subsequent cycle, navigator placed in middle of CINE train deciding about data from same cycle; **b** comparison of representative basal magnitude images between prospective (top) and center navigator (bottom)

For comparison, TPM acquisitions of basal slices were acquired with both navigator strategies in additional five volunteers. Subjective blinded image grading was performed by two independent, experienced observers with magnitude images. The image quality was scored for different heart phases (early systole, late systole, early diastole and late diastole) considering edge sharpness, blurring and motion artifacts: poor (1), fair (2), acceptable (3), good (4), excellent (5). For all measurements the width of the navigator window was set to ± 4.0 mm. The navigator duration was 12.2 ms. The additional time was considered in the determination of time to peak (TTP) velocity values in diastole.

Black blood optimization

A spatially selective preparation "sandwich"-shaped pulse [5] was applied every ~ 150 ms for saturation of the blood signal in the ventricular cavities to avoid blood flow related artifacts and to simplify segmentation of myocardial contours (Fig. 3). However, it has been shown in our preparatory work that the gap of 24 mm between the two saturation bands of the pulse as used for LV application in our previous work leads to a decreased signal of the basal RV wall. This was observed particularly in systolic frames due to the more pronounced long-axis shortening of the RV free wall compared to the LV wall. To analyze the impact of the gap on saturation effects, the gap of the saturation bands was varied between 20 and 36 mm in a basal slice for additional five

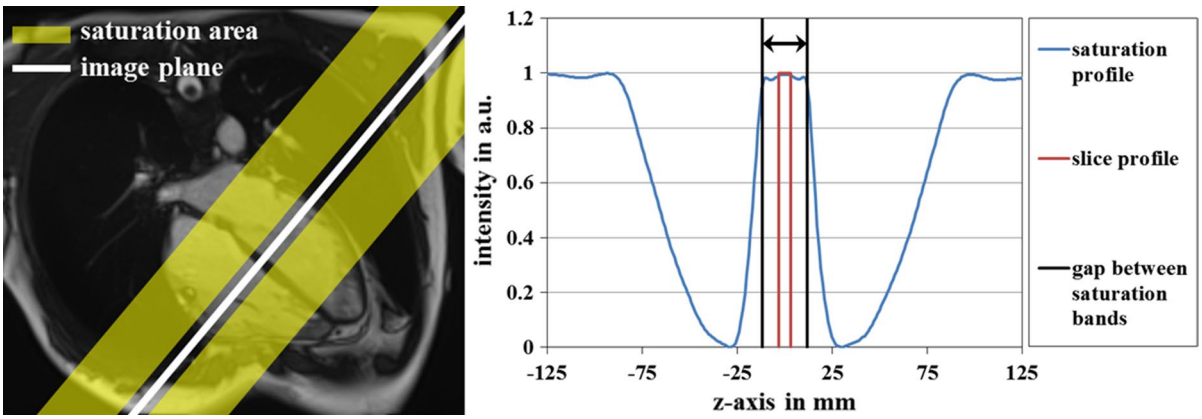

Fig. 3 Schematic representation of the black blood saturation (left) and the according measured saturation profile (right) with a gap size of 24 mm and the centered slice position (slice thickness 6 mm)

volunteers. For each gap size, SNR values were determined by the averaged signal of RV and LV regions (after segmentation of myocardial contours) and the standard deviation of a region of interest including only noise. To this end, one noise region was manually segmented in the first time frame of a dataset and used for all subsequent time frames.

Data post-processing

Data post-processing was performed using home-built software package in MATLAB (R2014a, Mathworks, Natick, MA, USA) to process automatically the phase-contrast MR velocity images. After eddy current correction by fitting a quadratic surface to the static tissue within the phase images [35], epi- and endocardial RV and LV contours were semi-automatically segmented [36]. Subsequently, the measured in-plane velocities (V_x, V_y) of RV and LV were transformed into velocity components oriented perpendicular (V_r) and circumferential (V_φ) to the endocardial contour (Fig. 1)—rather than calculating these components via a polar coordinate system with the center of gravity of the segmentation mask as presented in the past for the assessment of the LV, e.g. [5, 20].

Global velocity time courses of V_r, V_φ and V_z were quantified for RV and LV. Mean velocities for the LV time course were calculated for the entire LV segmentation mask including the septal wall, whereas the RV time course was determined only from the RV free wall. For segmental analysis, the LV was divided according to the American Heart Association (AHA) 16-segment model [37]. For the analysis of the RV, a 10-segment model as illustrated in Fig. 1 is proposed. The basal and the mid-ventricular RV slices were divided in four equally distributed segments (i.e. with equal distances along the endocardial contour) in consistency with the number of LV free wall segments of the AHA model. The apical RV plane was divided into two segments.

Additionally, systolic and diastolic peak velocities (Peak Sys/Dia) as well as time to peak (TTP Sys/Dia) values were derived from global and segmental V_r and V_z time courses. For V_φ, only the first two global peak velocities and corresponding TTPs for all three slices were determined according to Simpson et al. [24]. Although the second velocity peak of V_φ is still in systole, the peak velocity and corresponding TTP is referred to as V_φ Dia and TTP Dia for simplification (see upper right velocity time course in Fig. 6).

To show statistical differences, a Wilcoxon signed-rank test was used ($^*P < 0.05$, $^{**}P < 0.01$; Table 3) to compare global peak velocities and TTPs between RV and LV. Results of the segmental analysis are presented as bullseye plots (Fig. 1, right) permitting a direct comparison between the peak velocities/TTPs of different segments.

Furthermore, the amount of shortening (systole) and lengthening (diastole) $z_{\mathrm{sys/dia}}$ was determined by integrating global long-axis velocity $V_z(t)$ over time for both ventricles and each slice:

$$z_{\mathrm{sys/dia}} = \sum_{t \in \mathrm{sys/dia}} \left(V_z(t)\right) \cdot \Delta t$$

For a better visual representation and comparison, all time courses were normalized to end systole (as defined by the first minimum peak of the global radial basal LV velocities during diastole) prior to averaging over all volunteers (Fig. 6). This removes the timing variability between volunteers and makes the curves much easier to compare.

Results

Center navigator strategy

The comparison between the prospective and center navigator strategy is demonstrated in Fig. 2b and Table 1. For the prospective navigator, artefacts and blurring in early and late diastole due to respiratory motion are clearly visible. The subjective grading in Table 1 reveals a better overall image quality between the navigator strategies (2.8 ± 0.2 vs. 3.4 ± 0.4), as well as a better image quality in different heart phases.

Black blood optimization

Figure 4 demonstrates the impact of different gap sizes of the black blood saturation pulse. With a smaller gap between the two saturation bands, a reduced signal can be clearly observed. The reduction is most pronounced in regions with strong long-axis motion particularly in the free wall of the RV (green arrows Fig. 4). If the width is chosen too large, signal of blood-filled cavities is not suppressed sufficiently (red arrows Fig. 4), which may hinder a clear differentiation between blood and myocardium. The

Table 1 Image quality grading for the prospective and the center navigator strategy by two independent observers for different cardiac phases

	Subjective scoring mean values	
	Prospective	Center
Early systole	2.5 (1–4)	2.9 (2–4)
Late systole	3.1 (2–4)	3.6 (2–5)
Early diastole	2.9 (2–3)	3.5 (2–5)
Late diastole	2.8 (1–3)	3.8 (2–5)
Avaraged	2.8 ± 0.2	3.4 ± 0.4

Early systole, late systole, early diastole and late diastole: poor (1), fair (2), acceptable (3), good (4), excellent (5)

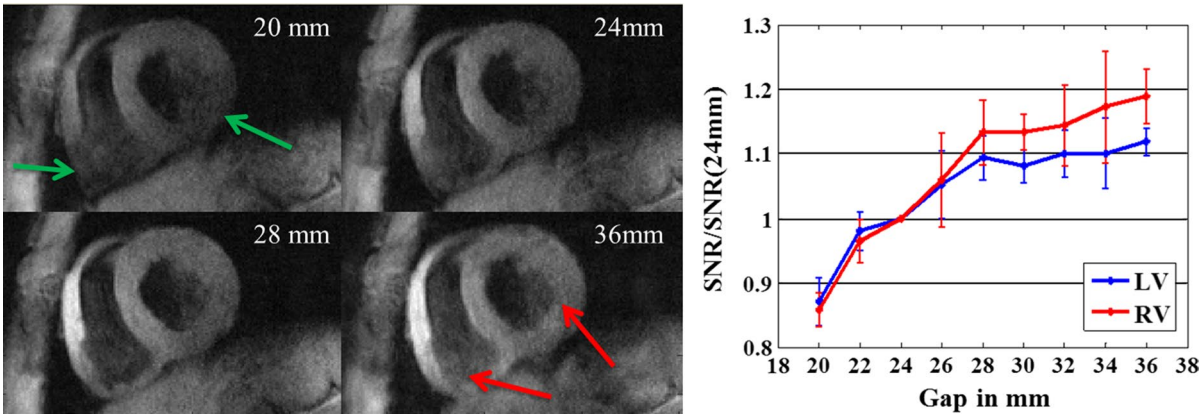

Fig. 4 Left: basal magnitude images of a representative volunteer with different gap sizes of the black blood saturation pulse; regions with strong long-axis motion suffer from signal loss due to saturation effects (green arrows). Too large gap widths result in insufficient blood saturation (red arrows); right: SNR averaged over the right and left myocardium and all time frames normalized to the SNR at gap size of 24 mm

graph (Fig. 4, right) shows SNR values averaged over all time frames and all five volunteers in relation to the SNR measured with a gap size of 24 mm (as used for the LV in previous studies) revealing an increase by more than 10% while increasing the gap by 4 mm. For systolic time frames with strong motion, a local SNR increase of more than 60% in the free heart wall of RV and LV without flow artefacts could be observed for gap sizes between 28 and 30 mm, which were used for the study measurements depending on the heart size.

Volunteer study

Standardized volumetric parameters are summarized in Table 2. The averaged TPM scan time per slice was 2.6 ± 0.5 min (navigator efficiency: 58.5%) and the averaged heart rate over all volunteers was 69 ± 14 bpm during the TPM measurements. Systolic and diastolic images of a basal slice of a representative volunteer are presented in Fig. 5 with overlaid pixel-wise color-coded long-axis velocities and vectors depicting the in-plane velocities. A synchronous

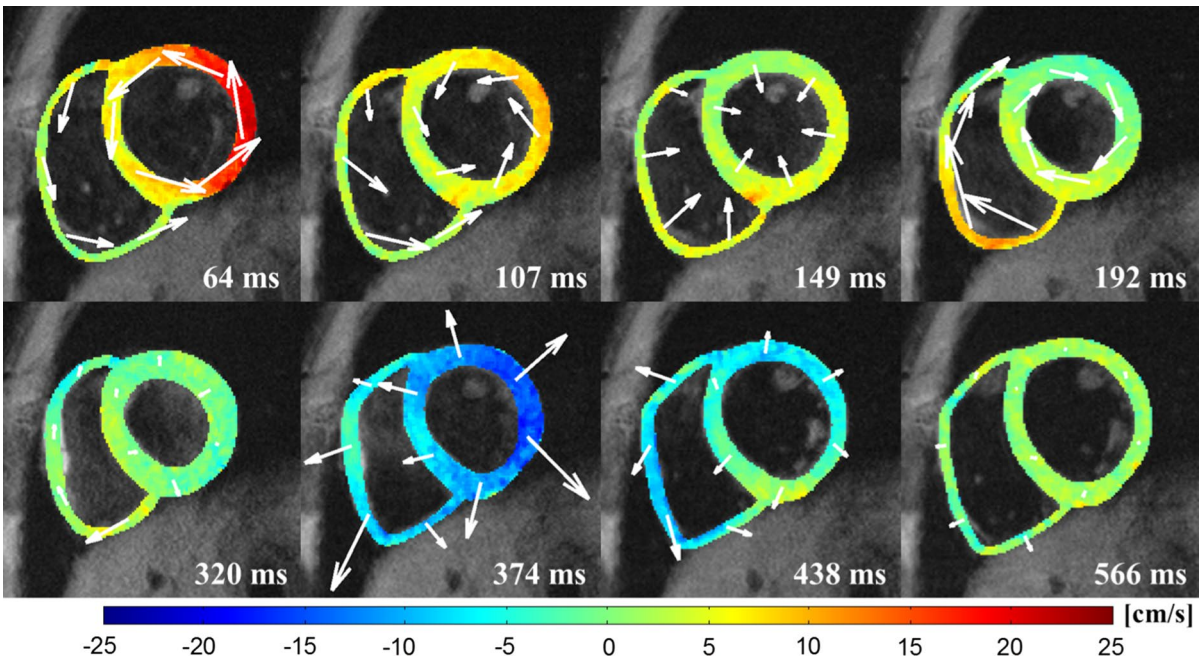

Fig. 5 Systolic and diastolic basal magnitude images of a representative volunteer with a pixel-wise color-coded long-axis velocities overlay and vectors proportional to the in-plane velocities for systole (top row) and diastole (bottom row)

Table 2 Standardized volumetric parameters from CINE CMR

	Mean ± STD
Mass in g	150.0 ± 38.8
LVESV in mL	52.6 ± 12.4
LVEDV in mL	143.4 ± 26.7
LVEF in %	62.8 ± 3.7
RVESV in mL	60.5 ± 40.5
RVEDV in mL	149.9 ± 17.3
RVEF in %	58.8 ± 7.1

LVESV left ventricular end systolic volume, *LVEDV* left ventricular end diastolic volume, *LVEF* left ventricular ejection fraction, *RVESV* right ventricular end systolic volume, *RVEDV* right ventricular end diastolic volume, *RVEF* right ventricular ejection fraction

motion between the RV and LV can be observed. The high spatial resolution enables a good delineation of the thin-walled RV (systole about 2–5 voxels and diastole about 3–8 voxels, Fig. 5) and its velocities. The overlays indicate a global long-axis and radial contraction and expansion in systole and diastole, as well as the clockwise and counter-clockwise rotation during systole for both ventricles. However, regional differences of myocardial motion during the heart cycle can also be observed. For instance, higher long-axis velocities in the LV free wall were seen compared to the RV free wall.

Global velocities

As shown in Fig. 6 and Table 3, the mean systolic radial peak velocities were significantly higher in the basal, mid-ventricular and apical parts of the RV free wall compared to the LV. In contrast, the RV diastolic radial peak velocities were only in the apical slice significantly lower compared to the LV. Systolic radial TTPs of the RV are significantly higher in all slice locations, whereas diastolic TTPs are significantly lower (Table 3).

Systolic and diastolic RV long-axis (V_z) peak velocities were significantly lower in all slices compared to the LV except the basal systolic peak velocity (Table 3). However, the shape of the RV velocity time course differed from the LV curves (Fig. 6). The LV exhibits one strong velocity peak during systole. In the RV, two velocity peaks can be observed with approximately the same amplitude. This also influences the determination of the global systolic V_z TTP, which shows a delay and much higher standard deviation compared to the LV (Table 3). Although systolic and diastolic LV V_z peak velocities are higher compared to the RV, a more pronounced RV shortening and lengthening (integral

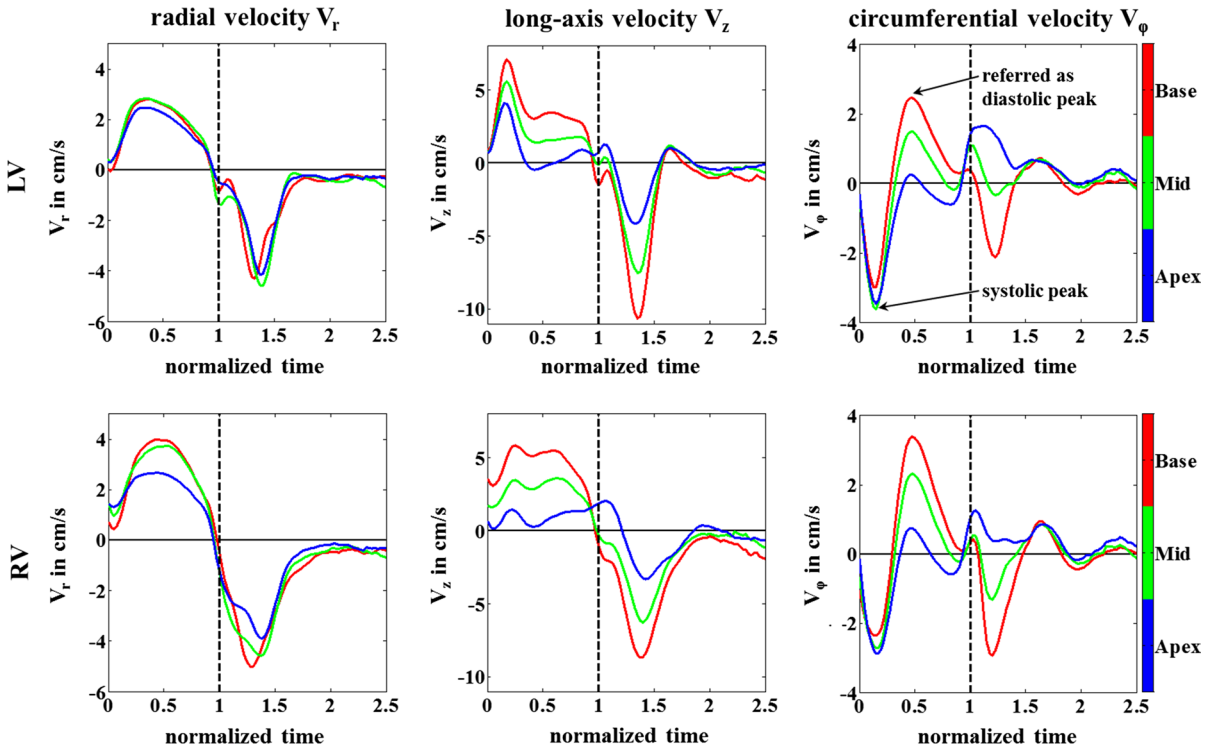

Fig. 6 Comparison of the global mean time courses of base, mid and apex for radial (left column) long-axis (center column) and circumferential velocities (right column) of the left (top row) and the right (bottom row) ventricle averaged over all volunteers

Table 3 Overview of global peak velocities and corresponding time to peak (TTP) velocities averaged over all volunteers

	Radial		Long-axis		Circumferential	
	LV	RV	LV	RV	LV	RV
Peak Sys in cm/s						
Base	2.8 ± 0.5	4.1 ± 0.6**	7.2 ± 1.3	6.4 ± 1.8	− 3.1 ± 0.9	− 2.7 ± 1.0*
Mid	2.9 ± 0.3	3.9 ± 0.6**	5.7 ± 1.3	4.1 ± 1.7**	− 3.8 ± 1.0	− 3.0 ± 1.0**
Apex	2.6 ± 0.4	3.0 ± 0.7**	4.2 ± 1.8	2.0 ± 1.6**	− 3.6 ± 0.8	− 3.1 ± 1.2**
Peak Dia in cm/s						
Base	− 5.0 ± 0.8	− 5.2 ± 0.7	− 11.7 ± 1.9	− 9.2 ± 1.7**	2.7 ± 0.8	3.7 ± 1.1**
Mid	− 5.1 ± 0.7	− 4.9 ± 0.6	− 8.7 ± 2.0	− 6.9 ± 1.4**	1.7 ± 0.7	2.5 ± 1.0**
Apex	− 5.0 ± 0.9	− 4.5 ± 0.9**	− 5.0 ± 1.9	− 4.1 ± 1.4**	0.4 ± 0.8	1.0 ± 1.0**
TTP Sys in ms						
Base	122 ± 26	143 ± 28**	63 ± 11	117 ± 54**	51 ± 12	56 ± 18
Mid	114 ± 25	153 ± 33**	63 ± 11	125 ± 58**	51 ± 9	58 ± 14
Apex	109 ± 25	142 ± 40**	57 ± 10	81 ± 29**	54 ± 10	59 ± 16
TTP Dia in ms						
Base	394 ± 33	383 ± 35**	406 ± 32	419 ± 27**	144 ± 18	146 ± 17
Mid	414 ± 31	399 ± 53**	412 ± 26	425 ± 25**	143 ± 18	144 ± 16
Apex	422 ± 28	418 ± 39*	400 ± 28	453 ± 81**	144 ± 17	143 ± 22

The stars denote significant differences between RV and LV of the corresponding slice location (*$P < 0.05$, **$P < 0.01$)

over V_z) was observed due to a wider width of the systolic and diastolic RV V_z time course (Fig. 6). Therefore, the averaged ratio z_{RV}/z_{LV} of the contraction (systole) and expansion (diastole) length exhibited a more pronounced through-plane motion of the RV in basal and mid-ventricular slices for systole and diastole (z_{RV}/z_{LV} systole: base 1.31 ± 0.22, mid 1.26 ± 0.28, apex 1.02 ± 0.61; diastole: base 1.29 ± 0.21, mid 1.28 ± 0.38, apex 1.01 ± 0.68). Diastolic V_z TTP of the RV were only slightly, but significantly, delayed (Table 3).

Circumferential velocities, V_φ, also showed a similar time course for LV and RV in all slices. Systolic peak velocities were significantly higher in the LV compared to the RV (Table 3). The second RV velocity peak of V_φ (referred to as diastolic peak) was significantly increased in all slices compared to the LV (Table 3). In all slices, TTPs of V_φ appeared synchronously without any significant differences between the ventricles (Table 3).

Segmental velocities

As an example, segmental basal radial and long-axis time courses averaged over all volunteers are shown in Fig. 7 revealing regional differences between LV and RV segments such as different timing and velocity distribution.

Systolic and diastolic radial, as well as long-axis peak velocities in the RV decreased from the free wall to the segments adjacent to the LV (Figs. 7 and 8). Similar to the LV, the highest peak radial and long-axis velocities in systole and diastole can be found in the basal segments of the RV and decrease towards apical segments. The maximum velocities were observed in the basal and mid-ventricular inferolateral segments of the RV free wall in our 10-segment RV model (base: radial sys/dia: 5.6 ± 0.9/− 8.4 ± 1.5, long-axis sys/dia: 8.0 ± 2.5/− 11.0 ± 2.2; mid: radial sys/dia: 5.4 ± 0.9/− 7.4 ± 1.5, long-axis sys/dia: 5.6 ± 2.0/− 8.6 ± 2.1; Fig. 8).

The segmental TTP analysis (Fig. 9) shows that the RV has a different timing compared to the synchronous LV behavior, which is supported by an increased standard deviation (std) when averaging over all segments: std TTP V_rLV/RV systole: 7.8/19.5 ms, diastole: 12.3/13.9 ms; std TTP V_z LV/RV systole: 4.0/12.2 ms, diastole: 5.5/13.5 ms. Shortest systolic radial TTPs can be found in basal inferior RV segments (Fig. 9). Longest systolic radial TTPs appear in lateral and anterior mid-ventricular RV segments, but essentially do not differ from corresponding basal segments. Systolic RV long-axis TTPs follow a counter-clockwise delay course. Highest TTP values are in the basal and mid-ventricular inferolateral and inferior segments and decrease towards apical segments. Diastolic radial and long-axis TTPs appear similar (Fig. 9). Shortest TTPs also occur in basal inferolateral and inferior RV segments and increase towards apical segments.

Discussion

RV function is an important parameter of cardiac prognosis. Diseases of the RV or lungs (e.g. arrhythmogenic right ventricular dysplasia, RV infarction, pulmonary hypertension), as well as LV pathologies (e.g. dilated cardiomyopathy) can

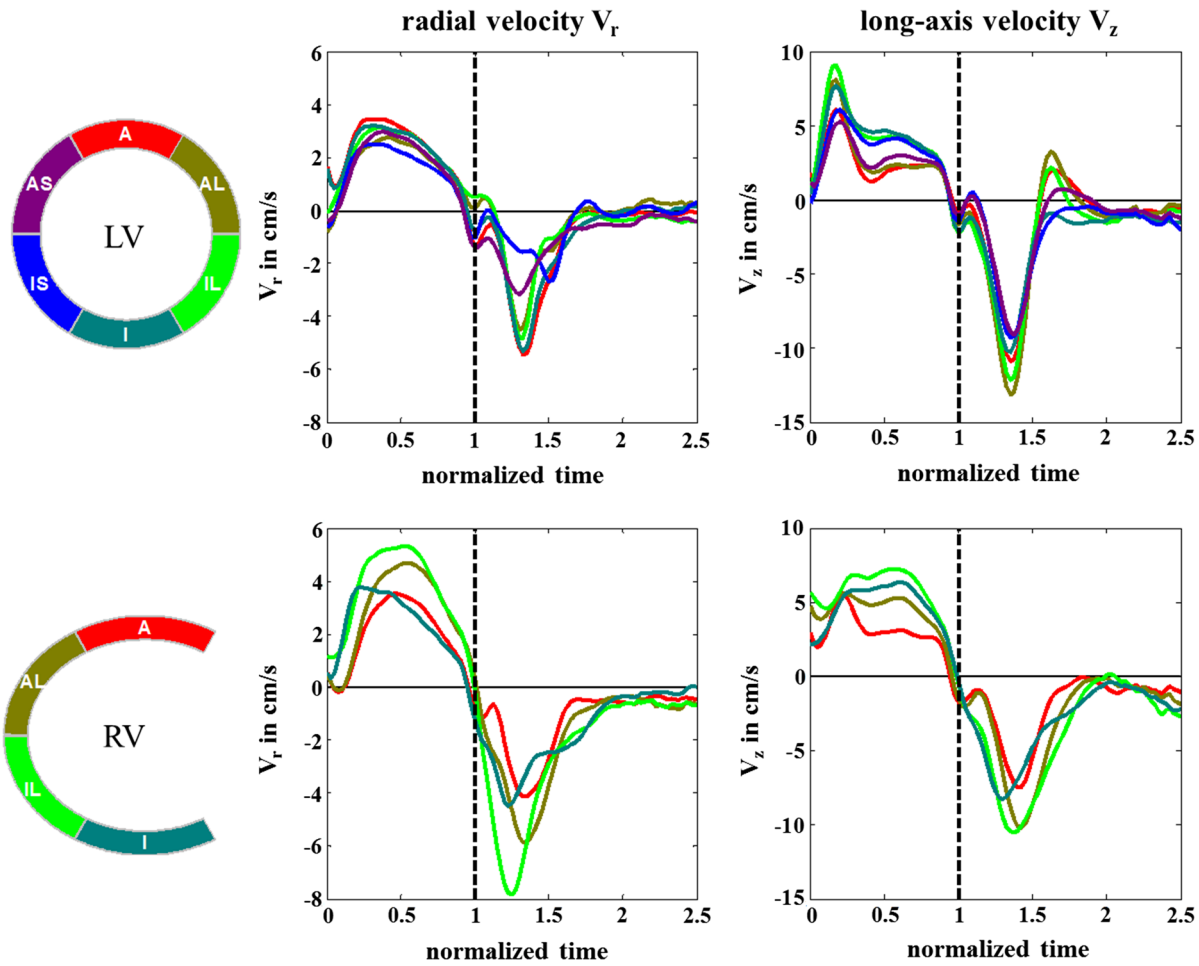

Fig. 7 Segmental mean time courses of basal slice for radial (left column) and long-axis velocities (right column) of the left (top row) and the right (bottom row) ventricle averaged over all volunteers

cause RV dysfunction. As LV and RV function are closely linked, the prognosis of patients with LV heart disease worsens with progressive RV failure [38].

In this work a robust TPM protocol for the acquisition of biventricular myocardial velocities with a high temporal resolution of 21.3 ms and high spatial resolution could be implemented and successfully applied in 25 healthy volunteers. The isotropic in-plane resolution of 1.0 mm enabled the analysis of the thin right ventricle.

Center navigator strategy

Despite the use of kt-based parallel imaging, the scan time (~ 92 s) considering a heart rate of 60 bpm and 100% navigator efficiency) exceeded a normal breath-hold capability (~ 16 s). Therefore, respiration control was necessary. With the implementation of the center navigator, motion artefacts could be substantially reduced in diastole. For individuals with very low heart rates and irregular breathing patterns, this strategy might also lead to respiratory artefacts in early systole and end diastole. The use of more advanced navigator strategies like double navigator, in which the navigator decision is based on navigator signals acquired before and at the end of the cardiac cycle, or multiple navigators, played out during the heart cycle, might enable a more accurate data acquisition. However, these techniques would also substantially increase the scan time due to lower acceptance rates [22]. Using additional biofeedback techniques in combination with a double navigator strategy [24] enable similar acceptance rates compared to our study, whereas difficulties are expected to image patients due to the level of compliance needed to use the respiratory trace to guide their own breathing [24].

The total scan time of ~ 8 min for all three short-axis slices is relatively long for clinical application. With more advanced acquisition strategies such as spiral trajectories, the scan time might be reduced to breath-hold tolerable duration with still adequate spatio-temporal resolution [7, 39].

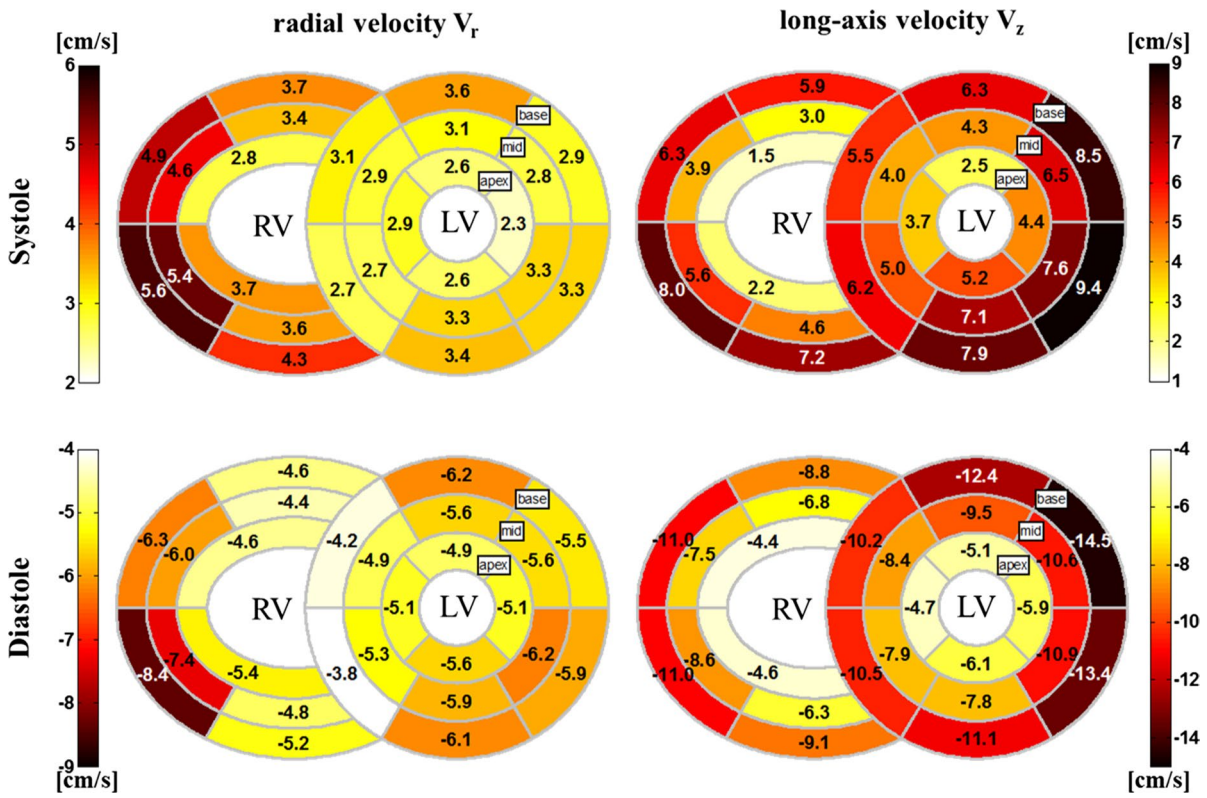

Fig. 8 Bullseye plots of systolic (top row) and diastolic (bottom row) radial (left) and long-axis (right) peak velocities averaged over all volunteers

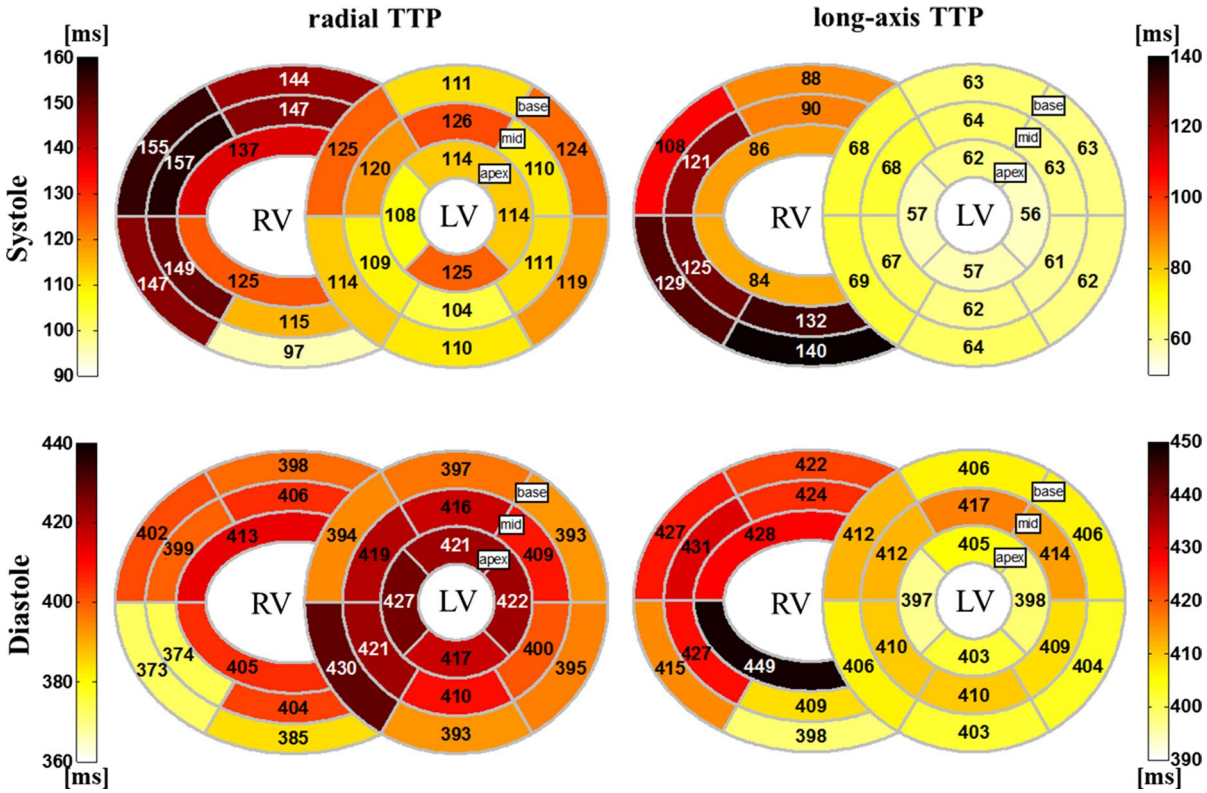

Fig. 9 Bullseye plots of systolic (top row) and diastolic (bottom row) radial and long-axis TTPs averaged over all volunteers

Black blood saturation

The optimization of the black blood saturation improved image quality and SNR and permitted sufficient blood suppression enabling a proper segmentation. Especially the signal in the lateral basal heart wall of RV and LV with strong long-axis motion could be significantly increased (Fig. 4).

Velocity analysis

Because of the different geometry of the RV compared to the LV, a new strategy was proposed to calculate radial and circumferential velocity components for both ventricles based on the endo-myocardial wall. We also compared global and segmental LV peak velocities and TTPs of the new calculation strategy presented here with the conventional LV calculation values using a paired *t* test. No significant differences could be observed ($P > 0.05$). All global and segmental LV peak velocities match also well with the LV velocities of a comparable age-matched group of Föll et al. [20]. Here, the LV velocity components were calculated based on polar coordinates and a lower spatial resolution was used. Corresponding TTP values also agree well which suggests that the temporal resolution of 21.3 ms (compared to 13.8 ms in [20]) is sufficient to capture the wall motion dynamics.

In addition to LV analysis, our TPM protocol allows a complete RV evaluation for base, mid and apex. Our results show that the RV function exhibits a more complex timing and segmental peak velocity distribution compared to the LV. Moreover, a more pronounced RV shortening and lengthening was observed—a fact that provoked the optimization of the black blood saturation pulse. Radial velocities were higher in the RV compared to the LV. High radial RV velocities might be explained by the predominantly transversal myocardial fiber orientation of the free RV wall [40]. Systolic TTPs were delayed in the RV compared to the LV. As the aortic valve closes before the pulmonary valve, the duration of systole is shorter in the LV compared to the RV and the measured TTP might reflect the delayed behavior of the cardiac cycle in the RV.

In line with literature, we found highest velocities in the long-axis direction of the RV [25]. In this study, a comparable distribution of mid-ventricular RV radial velocities was described. Our global RV mid-ventricular time courses are similar to Steeden et al. [41], whereas in our study velocity peak values were higher. Previous studies by Steeden et al. [41], with no segmental analysis, and by Kayser et al. [25] who divided the mid-ventricular RV slice in six segments, a 10-segment RV free wall model covering the whole heart based on the AHA 16-segment LV model was introduced to enable segmental analysis. Furthermore, additional features like the closure of the valves and more pronounced velocity peaks were observed. Additionally, scan time could be reduced from 8–9 min to 2.6 ± 0.5 min while increasing spatial as well as temporal resolution of about 40 and 22%, respectively, compared to Steeden et al. [41].

However, the studies of Kayser et al. and Steeden et al. [25, 41] did not include time to peak velocities and only a single mid-ventricular slice without blood saturation was acquired. Especially for basal short-axis acquisitions, where the blood flow is most pronounced, saturation is necessary to avoid flow artefacts.

Furthermore, we presented a comprehensive evaluation of global and segmental velocities, as well as the timing of the complete RV. To our knowledge, such an analysis was still missing in literature.

RV evaluation using echocardiography is limited due to restrictions of the acoustic window in many patients. Therefore, only regional lateral long-axis velocities for basal and mid-ventricular segments are commonly obtained from a four chamber view for the analysis of RV motion [42–44]. As TPM data are determined from fixed short-axis slices a direct comparison is difficult. However, the comparison of longitudinal RV peak velocity values between the control groups of these echocardiography studies [42–44] reveal strong deviations among each other.

MRI, in contrast, is the gold-standard for the evaluation of RV ejection fraction and offers the advantage of a quantitative, relatively examiner-independent and regional RV function analysis. Several methods such as MR tagging [45–48] or displacement encoding with stimulated echoes (DENSE) [49–51] were assessed for the evaluation of segmental three directional RV function by analyzing strain and strain rate. Compared to high resolution TPM, these methods exhibit a lower spatial (> 1.5 mm) [52] and temporal resolution (> 28 ms) [52]. MR tagging is additionally limited to the spatial raster size of the saturation grid (> 4 mm) [52]. These limitations might hamper the detection of local small differences in myocardial function of the thin RV due to partial volume effects.

Another possibility to determine strain or strain rate from CINE time series is called feature tracking (FT) [53] and was already successfully applied to the RV [54]. As only the contours of the myocardium are tracked over time, motion information is only obtained from the translation and deformation of the myocardial borders and not from the myocardium itself [55] as with tagging or TPM. Additionally, a recent study showed differences in strain measurements between two types of FT solutions [56].

Strong relations between velocities and myocardial function have been reported in previous literature, for example, a correlation between systolic long-axis and rotational velocities and myocardial contractility [57], as well as between early diastolic velocities and active diastolic function [58, 59]. Furthermore, the evaluation of LV synchrony, which relies on a highly time-resolved evaluation of segmental

ventricular motion, has gained increased importance for the management of patients with dyssynchrony. Such patients may in particular benefit from a robust and comprehensive biventricular motion analysis based on TPM velocities—promising results have already been presented for the LV [31, 60]. Moreover, an echocardiography study by Thorstensen et al. [61] reported that velocity parameters were more sensitive in detecting contraction changes of the LV than strain.

Our proposed TPM method provides high temporal and spatial resolution velocity maps even of the thin RV. TPM acquisitions also inherently include information on deformation due to the relation of deformation/strain and velocity (i.e. time integral of velocity yields displacement, deformation is derived from the spatial variation of displacement), as used for TDI-based strain analysis as well as for previous TPM studies [62–64]. In situations of very small spatially localized changes in myocardial function the acquired three short-axis slices might not be sufficient and strain based methods covering the whole heart might be more sensitive.

However, the sensitivity of these strain based methods in the detection of small changes in myocardial RV motion in comparison to high resolution TPM velocities and/or TPM derived strain has to be further investigated.

Conclusion

High spatio-temporal resolution TPM implemented in this work enables a detailed biventricular analysis of myocardial motion and might provide a reliable tool for description and detection of diseases affecting left and right ventricular function. With the advantages of high spatio-temporal resolution, examiner-independency and possibility for a segmental evaluation, our pilot study on TPM MRI of the RV in healthy volunteers might serve as a base for multi-center studies of biventricular function in patients. Further work should include gender- and age-related analysis, as well as an extended analysis of the complex timing between RV and LV to extrapolate comprehensive inter- and intraventricular synchronicity parameters.

Acknowledgements We would like to thank Alexandra Mannweiler for recruiting volunteers and Adriana Komancsek for assistance in performing the MR examinations.

Grand support This research was supported by the Deutsche Forschungsgemeinschaft (DFG), Grant FO 507/3-1.

Author contribution MM: Protocol/project development, Data collection or management, Data analysis; DF: Protocol/project development, Data collection or management, Data analysis; JH: Protocol/project development; BJ: Protocol/project development, Data collection or management, Data analysis.

Compliance with ethical standards

Conflict of interest The authors declare that they have no conflict of interest.

Ethical approval All procedures performed in studies involving human participants were in accordance with the ethical standards of the institutional and/or national research committee and with the 1964 Helsinki declaration and its later amendments or comparable ethical standards.

Informed consent Informed consent was obtained from all individual participants included in the study.

References

1. Apostolakis S, Konstantinides S (2012) The right ventricle in health and disease: insights into physiology, pathophysiology and diagnostic management. Cardiology 121:263–273
2. Teske AJ, Cox MG, De Boeck BW, Doevendans PA, Hauer RN, Cramer MJ (2009) Echocardiographic tissue deformation imaging quantifies abnormal regional right ventricular function in arrhythmogenic right ventricular dysplasia/cardiomyopathy. J Am Soc Echocardiogr 22:920–927
3. Vitarelli A, Franciosa P, Nguyen BL, Capotosto L, Ciccaglioni A, Conde Y, Iorio G, De Curtis G, Caranci F, Vitarelli M, Lucchetti P, Dettori O, De Cicco V (2011) Additive value of right ventricular dyssynchrony indexes in predicting the success of cardiac resynchronization therapy: a Speckle-Tracking Imaging Study. J Card Fail 17:392–402
4. Wang J, Prakasa K, Bomma C, Tandri H, Dalal D, James C, Tichnell C, Corretti M, Bluemke D, Calkins H, Abraham TP (2007) Comparison of novel echocardiographic parameters of right ventricular function with ejection fraction by cardiac magnetic resonance. J Am Soc Echocardiogr 20:1058–1064
5. Hennig J, Schneider B, Peschl S, Markl M, Laubenberger TKJ (1998) Analysis of myocardial motion based on velocity measurements with a black blood prepared segmented gradient-echo sequence: methodology and applications to normal volunteers and patients. J Magn Reson Imaging 8:868–877
6. Petersen SE, Jung BA, Wiesmann F, Selvanayagam JB, Francis JM, Hennig J, Neubauer S, Robson MD (2006) Myocardial tissue phase mapping with cine phase-contrast MR Imaging: regional wall motion analysis in healthy volunteers. Radiology 238:816–826
7. Menza, Marius, Föll D, Hennig J, Jung B (2016) Spiral SPIRIT tissue phase mapping enables the acquisition of myocardial motion with high temporal and spatial resolution during breathhold. Proc. 24th Annu. Meet. ISMRM. Singapore, p 3131
8. von Knobelsdorff-Brenkenhoff F, Hennig P, Menza M, Dieringer MA, Foell D, Jung B, Schulz-Menger J (2016) Myocardial dysfunction in patients with aortic stenosis and hypertensive heart disease assessed by MR tissue phase mapping. J Magn Reson Imaging 44:168–177
9. Delfino JG, Bhasin M, Cole R, Eisner RL, Merlino J, Leon AR, Oshinski JN (2006) Comparison of myocardial velocities obtained with magnetic resonance phase velocity mapping and tissue doppler imaging in normal subjects and patients with left ventricular dyssynchrony. J Magn Reson Imaging 24:304–311
10. Paelinck BP, de Roos A, Bax JJ, Bosmans JM, van Der Geest RJ, Dhondt D, Parizel PM, Vrints CJ, Lamb HJ (2005) Feasibility of tissue magnetic resonance imaging. J Am Coll Cardiol 45:1109–1116

11. Marsan NA, Westenberg JJM, Tops LF, Ypenburg C, Holman ER, Reiber JHC, de Roos A, van der Wall EE, Schalij MJ, Roelandt JR, Bax JJ (2008) Comparison between tissue Doppler imaging and velocity-encoded magnetic resonance imaging for measurement of myocardial Velocities, assessment of left ventricular dyssynchrony, and estimation of left ventricular filling pressures in patients with ischemic cardiomyopathy. Am J Cardiol 102:1366–1372
12. Jung B, Schneider B, Markl M, Saurbier B, Geibel A, Hennig J (2004) Measurement of left ventricular velocities: phase contrast MRI velocity mapping versus tissue-Doppler-ultrasound in healthy volunteers. J Cardiovasc Magn Reson 6:777–783
13. Sandstede J, Lipke C, Beer M, Hofmann S, Pabst T, Kenn W, Neubauer S, Hahn D (1999) Age- and gender-specific differences in left and right ventricular cardiac function and mass determined by cine magnetic resonance imaging. Eur Radiol 10:438–442
14. Dong SJ, MacGregor JH, Crawley AP, McVeigh E, Belenkie I, Smith ER, Tyberg JV, Beyar R (1994) Left ventricular wall thickness and regional systolic function in patients with hypertrophic cardiomyopathy. A three-dimensional tagged magnetic resonance imaging study. Circulation 90:1200–1209
15. Fisher M, von Schulthess G, Higgins C (1985) Multiphasic cardiac magnetic resonance imaging: normal regional left ventricular wall thickening. Am J Roentgenol 145:27–30
16. Schneider B, Markl M, Geiges C, Winterer J, Thuerl C, Laubenberger J, Hennig J, Langer M (2001) Cardiac phase contrast gradient echo MRI characterization of abnormal left ventricular wall motion in patients with ischemic heart disease. [Miscellaneous Article]. J Comput Assist Tomogr 25:550–557
17. Steeden JA, Kowalik GT, Taylor A, Muthurangu V (2014) Tissue phase mapping using breath-hold 4D PCMR. J Cardiovasc Magn Reson 16:W30
18. Föll D, Jung B, Staehle F, Schilli E, Bode C, Hennig J, Markl M (2009) Visualization of multidirectional regional left ventricular dynamics by high-temporal-resolution tissue phase mapping. J Magn Reson Imaging 29:1043–1052
19. Bauer S, Markl M, Föll D, Russe M, Stankovic Z, Jung B (2013) K-t GRAPPA accelerated phase contrast MRI: improved assessment of blood flow and 3-directional myocardial motion during breath-hold. J Magn Reson Imaging 38:1054–1062
20. Föll D, Jung B, Schilli E, Staehle F, Geibel A, Hennig J, Bode C, Markl M (2010) Magnetic resonance tissue phase mapping of myocardial motion new insight in age and gender. Circ Cardiovasc Imaging 3:54–64
21. Jung B, Markl M, Föll D, Hennig J (2006) Investigating myocardial motion by MRI using tissue phase mapping. Eur J Cardiothorac Surg 29:S150–S157
22. Jung B, Zaitsev M, Hennig J, Markl M (2006) Navigator gated high temporal resolution tissue phase mapping of myocardial motion. Magn Reson Med 55:937–942
23. Jung B, Föll D, Böttler P, Petersen S, Hennig J, Markl M (2006) Detailed analysis of myocardial motion in volunteers and patients using high-temporal-resolution MR tissue phase mapping. J Magn Reson Imaging 24:1033–1039
24. Simpson R, Keegan J, Firmin D (2013) Efficient and reproducible high resolution spiral myocardial phase velocity mapping of the entire cardiac cycle. J Cardiovasc Magn Reson 15:34
25. Kayser MDHWM, van der Geest Msc RJ, van der Wall MDEE, Duchateau Msc C, de Roos MDA (2000) Right ventricular function in patients after acute myocardial infarction assessed with phase contrast MR velocity mapping encoded in three directions. J Magn Reson Imaging 11:471–475
26. Matsukubo H, Matsuura T, Endo N, Asayama J, Watanabe T (1977) Echocardiographic measurement of right ventricular wall thickness. A new application of subxiphoid echocardiography. Circulation 56:278–284
27. Lang RM, Bierig M, Devereux RB, Flachskampf FA, Foster E, Pellikka PA, Picard MH, Roman MJ, Seward J, Shanewise J, Solomon S, Spencer KT, Sutton MSJ, Stewart W (2006) Recommendations for chamber quantification. Eur Heart J Cardiovasc Imaging 7:79–108
28. Jurcut R, Giusca S, Gerche AL, Vasile S, Ginghina C, Voigt J-U (2010) The echocardiographic assessment of the right ventricle: what to do in 2010? Eur Heart J Cardiovasc Imaging 11:81–96
29. Lutz A, Bornstedt A, Manzke R, Nienhaus GU, Etyngier P, Rasche V (2011) SAR reduced black-blood cine TPM for increased temporal resolution at 3T. Magn Reson Mater Phy Biol Med 24:127–135
30. Lutz A, Bornstedt A, Manzke R, Etyngier P, Nienhaus GU, Rottbauer W, Rasche V (2011) Acceleration of tissue phase mapping with sensitivity encoding at 3T. J Cardiovasc Magn Reson 13:59
31. Markl M, Schneider B, Hennig J (2002) Fast phase contrast cardiac magnetic resonance imaging: improved assessment and analysis of left ventricular wall motion. J Magn Reson Imaging 15:642–653
32. Codreanu I, Pegg TJ, Selvanayagam JB, Robson MD, Rider OJ, Dasanu CA, Jung BA, Taggart DP, Golding SJ, Clarke K, Holloway CJ (2014) Normal values of regional and global myocardial wall motion in young and elderly individuals using navigator gated tissue phase mapping. AGE 36:231–241
33. Jung B, Ullmann P, Honal M, Bauer S, Hennig J, Markl M (2008) Parallel MRI with extended and averaged GRAPPA kernels (PEAK-GRAPPA): optimized spatiotemporal dynamic imaging. J Magn Reson Imaging 28:1226–1232
34. Markl M, Harloff A, Bley TA, Zaitsev M, Jung B, Weigang E, Langer M, Hennig J, Frydrychowicz A (2007) Time-resolved 3D MR velocity mapping at 3T: improved navigator-gated assessment of vascular anatomy and blood flow. J Magn Reson Imaging 25:824–831
35. Walker PG, Cranney GB, Scheidegger MB, Waseleski G, Pohost GM, Yoganathan AP (1993) Semiautomated method for noise reduction and background phase error correction in MR phase velocity data. J Magn Reson Imaging 3:521–530
36. Lee ETY (1989) Choosing nodes in parametric curve interpolation. Comput Aided Des 21:363–370
37. Cerqueira MD, Weissman NJ, Dilsizian V, Jacobs AK, Kaul S, Laskey WK, Pennell DJ, Rumberger JA, Ryan T, Verani MS, Imaging AHAWG on MS and R for C (2002) Standardized myocardial segmentation and nomenclature for tomographic imaging of the heart. Circulation 105:539–542
38. Schwarz K, Singh S, Dawson D, Frenneaux MP (2013) Right ventricular function in left ventricular disease: pathophysiology and implications. Heart Lung Circ 22:507–511
39. Simpson R, Keegan J, Gatehouse P, Hansen M, Firmin D (2014) Spiral tissue phase velocity mapping in a breath-hold with non-cartesian SENSE. Magn Reson Med 72:659–668
40. Buckberg G, Hoffman JIE (2014) Right ventricular architecture responsible for mechanical performance: unifying role of ventricular septum. J Thorac Cardiovasc Surg 148(3166–3171):e4
41. Steeden JA, Knight DS, Bali S, Atkinson D, Taylor AM, Muthurangu V (2014) Self-navigated tissue phase mapping using a golden-angle spiral acquisition—proof of concept in patients with pulmonary hypertension. Magn Reson Med 71:145–155
42. Nikitin NP, Witte KKA, Thackray SDR, de Silva R, Clark AL, Cleland JGF (2003) Longitudinal ventricular function: normal values of atrioventricular annular and myocardial velocities measured with quantitative two-dimensional color doppler tissue imaging. J Am Soc Echocardiogr 16:906–921
43. Lindqvist P, Waldenström A, Henein M, Mörner S, Kazzam E (2005) Regional and global right ventricular function in healthy individuals aged 20–90 years: a pulsed Doppler Tissue Imaging

Study Umeå General Population Heart Study. Echocardiography 22:305–314
44. Pirat B, McCulloch ML, Zoghbi WA (2006) Evaluation of global and regional right ventricular systolic function in patients with pulmonary hypertension using a novel speckle tracking method. Am J Cardiol 98:699–704
45. Fayad ZA, Ferrari VA, Kraitchman DL, Young AA, Palevsky HI, Bloomgarden DC, Axel L (1998) Right ventricular regional function using MR tagging: normals versus chronic pulmonary hypertension. Magn Reson Med 39:116–123
46. Khalaf A, Tani D, Tadros S, Madan S (2013) Right- and Left-ventricular strain evaluation in repaired pediatric tetralogy of fallot patients using magnetic resonance tagging. Pediatr Cardiol 34:1206–1211
47. Nagao M, Yamasaki Y, Yonezawa M, Matsuo Y, Kamitani T, Yamamura K, Sakamoto I, Abe K, Kawanami S, Honda H (2015) Interventricular dyssynchrony using tagging magnetic resonance imaging predicts right ventricular dysfunction in adult congenital heart disease. Congenit Heart Dis 10:271–280
48. Naito H, Arisawa J, Harada K, Yamagami H, Kozuka T, Tamura S (1995) Assessment of right ventricular regional contraction and comparison with the left ventricle in normal humans: a cine magnetic resonance study with presaturation myocardial tagging. Br Heart J 74:186–191
49. Auger DA, Zhong X, Epstein FH, Spottiswoode BS (2012) Mapping right ventricular myocardial mechanics using 3D cine DENSE cardiovascular magnetic resonance. J Cardiovasc Magn Reson 14:4
50. Spottiswoode BS, Zhong X, Lorenz CH, Mayosi BM, Meintjes EM, Epstein FH (2008) 3D myocardial tissue tracking with slice followed cine DENSE MRI. J Magn Reson Imaging 27:1019–1027
51. Gilliam AD, Epstein FH (2013) Motion guided segmentation of the right ventricle for 3D cine DENSE MRI. J Cardiovasc Magn Reson 15:P82
52. Simpson RM, Keegan J, Firmin DN (2013) MR assessment of regional myocardial mechanics. J Magn Reson Imaging 37:576–599
53. Hor KN, Baumann R, Pedrizzetti G, Tonti G, Gottliebson WM, Taylor M, Benson W, Mazur W (2011) Magnetic resonance derived myocardial strain assessment using feature tracking. J Vis Exp. https://doi.org/10.3791/2356
54. Moon TJ, Choueiter N, Geva T, Valente AM, Gauvreau K, Harrild DM (2015) Relation of biventricular strain and dyssynchrony in repaired tetralogy of fallot measured by cardiac magnetic resonance to death and sustained ventricular tachycardia. Am J Cardiol 115:676–680
55. Schuster A, Hor KN, Kowallick JT, Beerbaum P, Kutty S (2016) Cardiovascular magnetic resonance myocardial feature tracking. Circ Cardiovasc Imaging 9:e004077
56. Schuster A, Stahnke V-C, Unterberg-Buchwald C, Kowallick JT, Lamata P, Steinmetz M, Kutty S, Fasshauer M, Staab W, Sohns JM, Bigalke B, Ritter C, Hasenfuß G, Beerbaum P, Lotz J (2015) Cardiovascular magnetic resonance feature-tracking assessment of myocardial mechanics: intervendor agreement and considerations regarding reproducibility. Clin Radiol 70:989–998
57. Lindqvist P, Waldenström A, Wikström G, Kazzam E (2007) Potential use of isovolumic contraction velocity in assessment of left ventricular contractility in man: a simultaneous pulsed Doppler tissue imaging and cardiac catheterization study. Eur J Echocardiogr 8:252–258
58. Nagueh SF, Middleton KJ, Kopelen HA, Zoghbi WA, Quiñones MA (1997) Doppler tissue imaging: a noninvasive technique for evaluation of left ventricular relaxation and estimation of filling pressures. J Am Coll Cardiol 30:1527–1533
59. Dong S-J, Hees PS, Siu CO, Weiss JL, Shapiro EP (2001) MRI assessment of LV relaxation by untwisting rate: a new isovolumic phase measure of τ. Am J Physiol Heart Circ Physiol 281:H2002–H2009
60. Delfino JG, Fornwalt BK, Eisner RL, Leon AR, Oshinski JN (2008) Cross-correlation delay to quantify myocardial dyssynchrony from phase contrast magnetic resonance (PCMR) velocity data. J Magn Reson Imaging 28:1086–1091
61. Thorstensen A, Dalen H, Amundsen BH, Støylen A (2011) Peak systolic velocity indices are more sensitive than end-systolic indices in detecting contraction changes assessed by echocardiography in young healthy humans. Eur Heart J Cardiovasc Imaging 12:924–930
62. Delfino JG, Fornwalt BK, Eisner RL, Leon AR, Oshinski JN (2008) Determination of transmural, endocardial, and epicardial radial strain and strain rate from phase contrast MR velocity data. J Magn Reson Imaging 27:522–528
63. Haraldsson H, Wigström L, Lundberg M, Bolger AF, Engvall J, Ebbers T, Kvitting J-PE (2008) Improved estimation and visualization of two-dimensional myocardial strain rate using MR velocity mapping. J Magn Reson Imaging 28:604–611
64. Lutz A, Paul J, Bornstedt A, Nienhaus GU, Etyngier P, Bernhardt P, Rottbauer W, Rasche V (2012) Volumetric motion quantification by 3D tissue phase mapped CMR. J Cardiovasc Magn Reson 14:1–13